Supporting Information

Synergistic DFT and Machine Learning Screening of Z-Scheme g-SiC/TMD Heterostructures for Efficient Overall Water Splitting

Wenxue Zhang[a],Yu Jiang[a], Jiuran Wen[a], Yajie Guo[a], Cheng He[b*]

a School of Materials Science and Engineering, Chang'an University, Xi'an 710064, China

b State Key Laboratory for Mechanical Behavior of Materials, School of Materials Science and Engineering, Xi'an Jiaotong University, Xi'an 710049, China

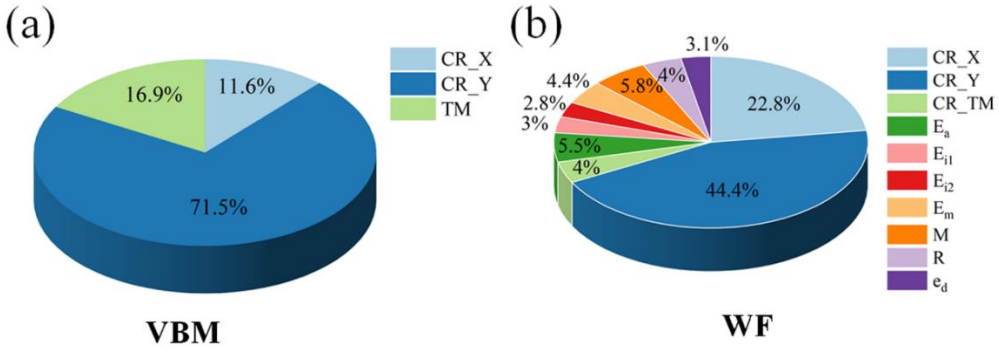

Figure S1. Feature importance associated with a) VBM and b) WF.

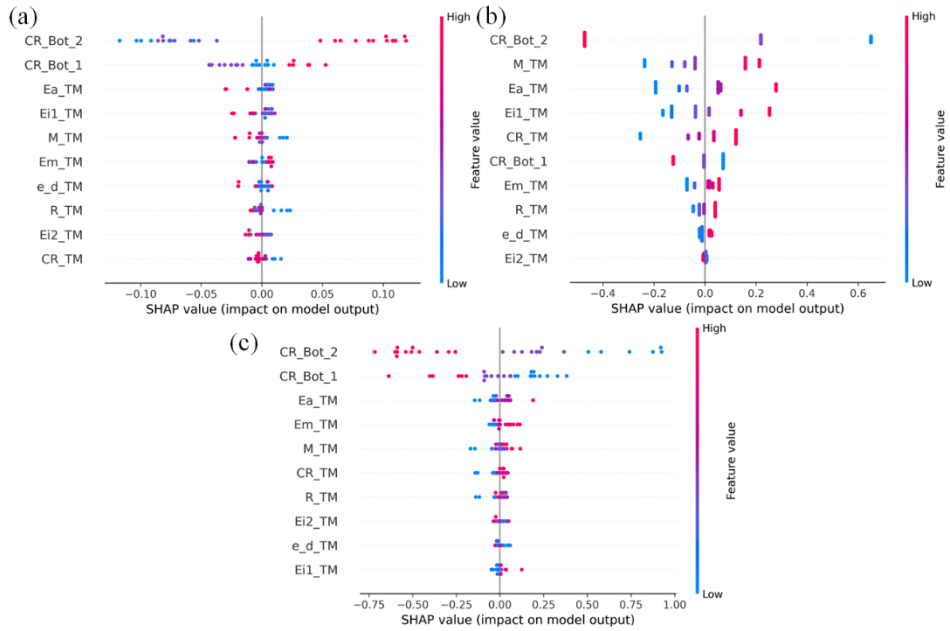

Figure S2. SHAP analysis plots of the selected features for the VBM (a), CBM (b), and WF (c) models. (CR_Bot_1 is CR_X; CR_Bot_2 is CR_Y)

*Corresponding Authors: Cheng He (hecheng@mail.xjtu.edu.cn)

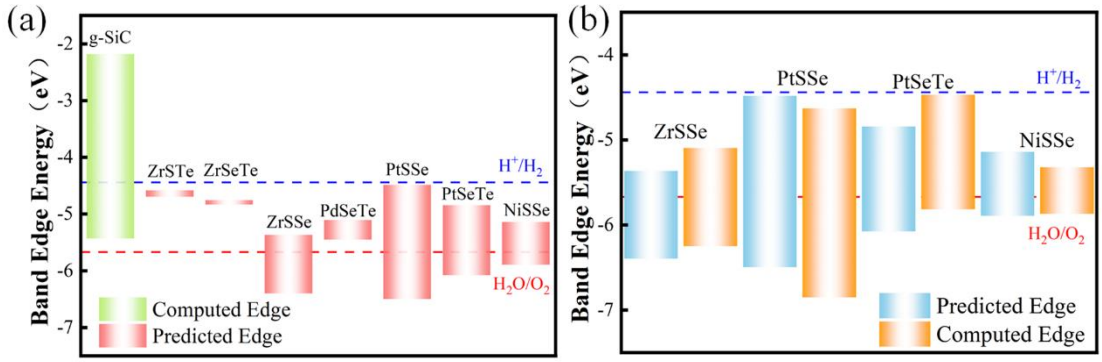

Figure S3. a) DFT-calculated band edge positions of g-SiC aligned with the ML-predicted band edge positions of some 1T-TMD monolayers. b) Comparison between the ML-predicted and DFT-calculated band edge positions for some 1T-TMD monolayers.

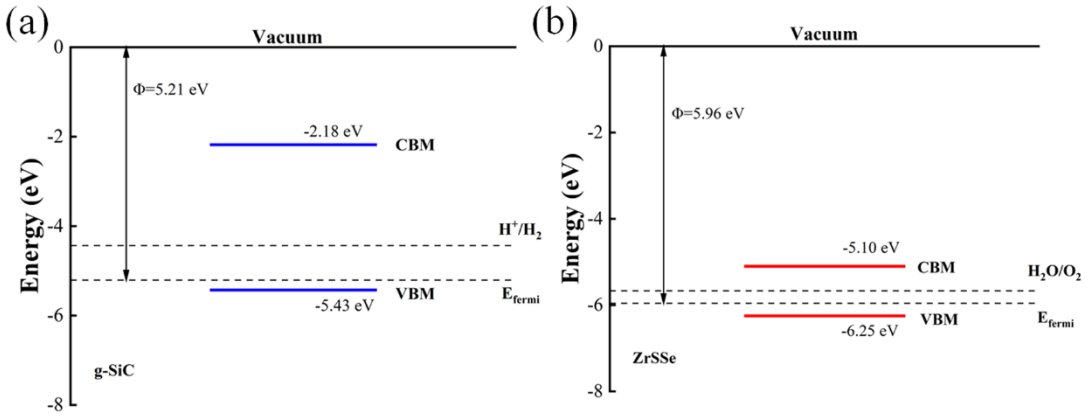

Figure S4. Band edge positions of a) g-SiC monolayer and b) ZrSSe monolayer.

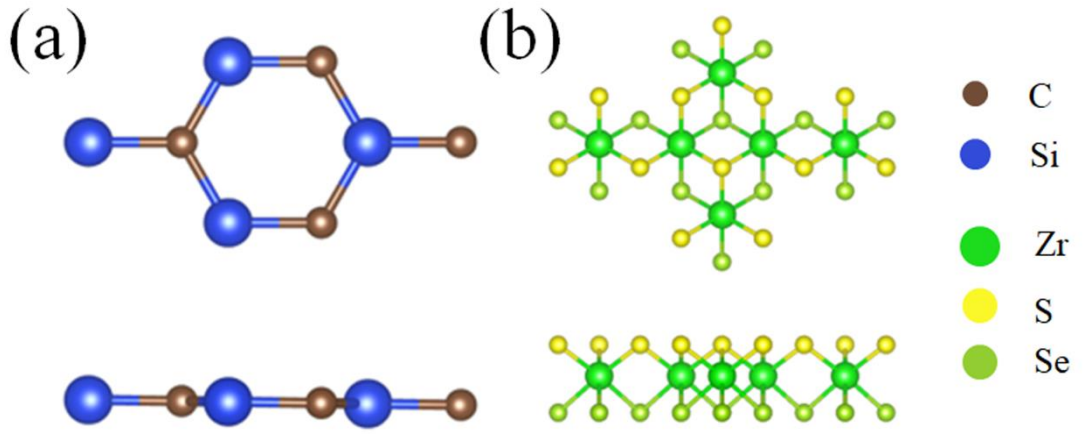

Figure S5. Schematic illustrations of the atomic structures for a) g-SiC monolayer and b) ZrSSe monolayer.

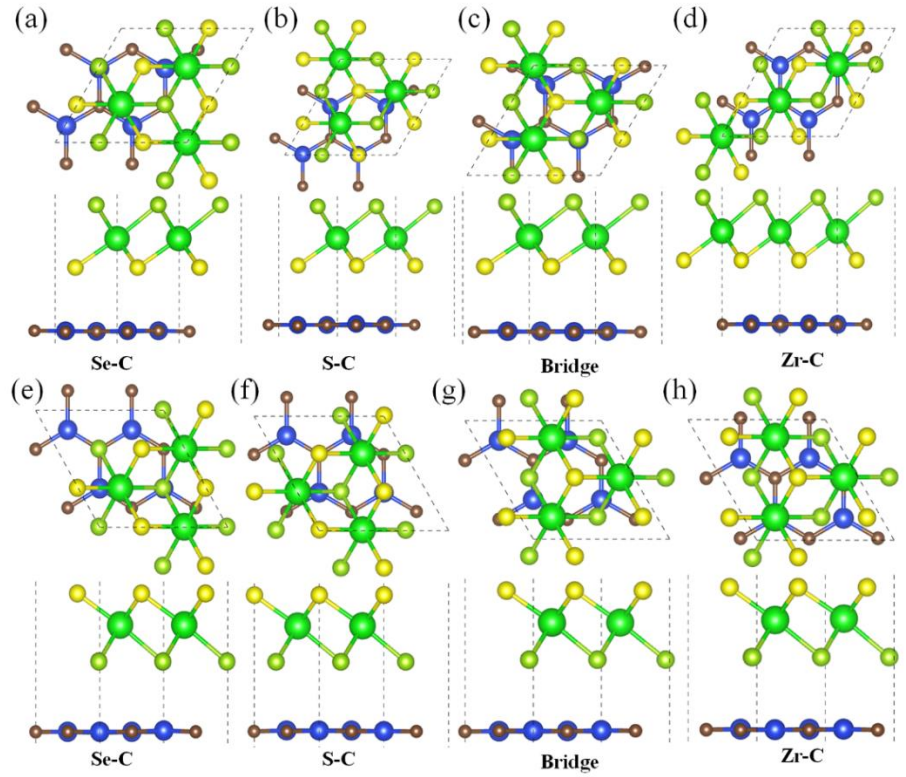

Figure S6. Schematic illustrations of the heterostructures. Se-C (a), S-C (b), Bridge (c), and Zr-C (d) stacking configurations of the g-SiC/SZrSe heterojunction. Se-C (e), S-C (f), Bridge (g), and Zr-C (h) stacking configurations of the g-SiC/SeZrS heterojunction.

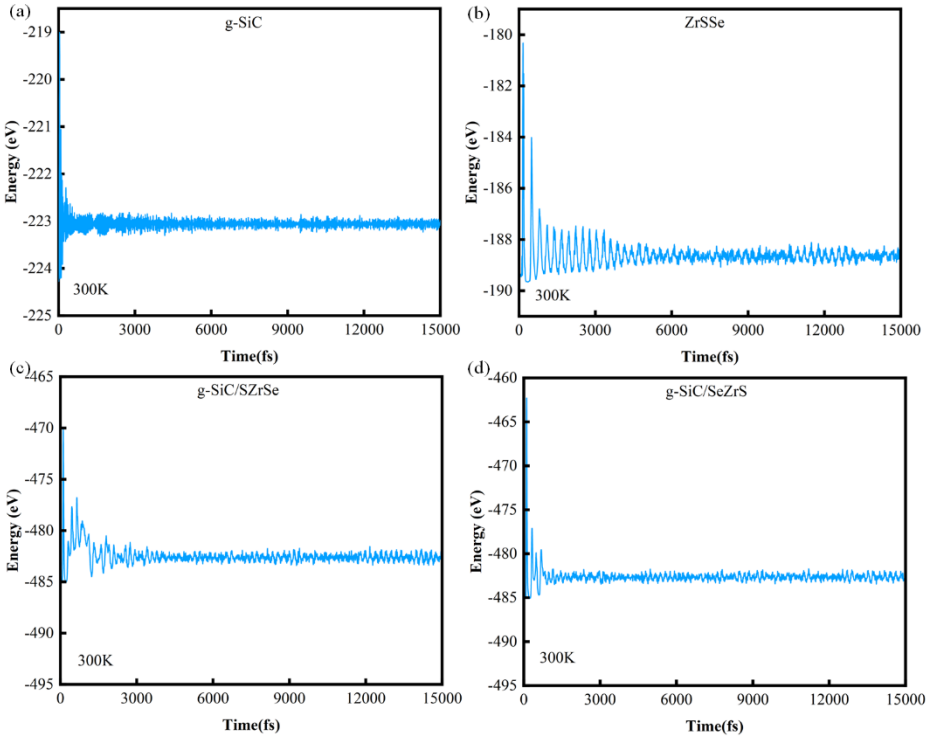

Figure S7. Figure 8. Ab initio molecular dynamics (AIMD) simulations of g-SiC (a)、ZrSSe (b)、g-SiC/SZrSe (c) and g-SiC/SeZrS (d)

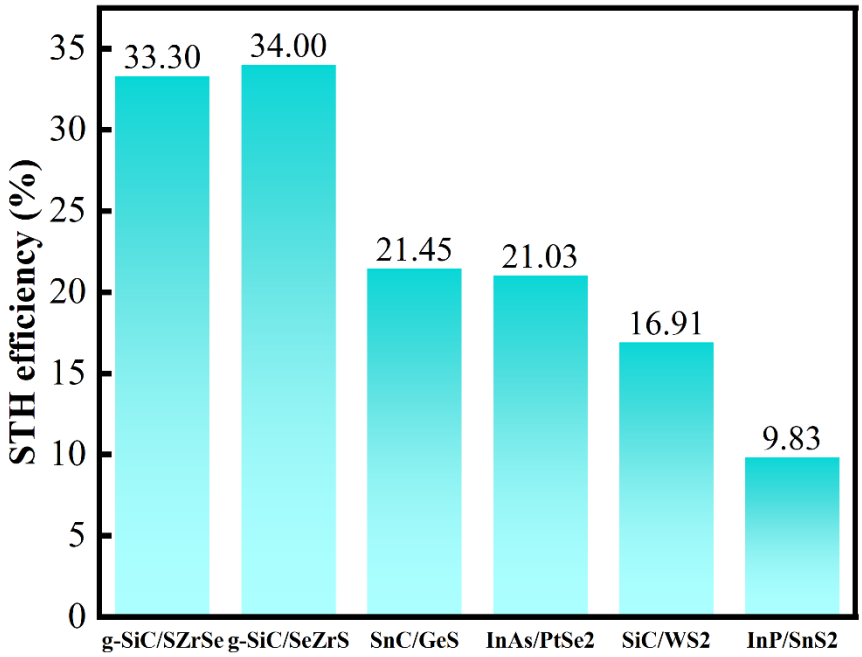

Figure S8. Comparison of the STH efficiencies of g-SiC/SZrSe and g-SiC/SeZrS heterojunctions with those of other reported heterojunctions.[1-4]

Table S1. The CBM, VBM, and WF values of 26 types of 1T-TMDs.

Materials	CBM (eV)	VBM (eV)	WF (eV)
PdTe2	0.1360	-0.1193	4.490
PdS2	1.5116	-0.2446	6.483
PdSe2	0.7920	-0.2386	5.494
HfSSe	1.3676	-0.2069	6.102
HfS2	1.5497	-0.3384	6.627
HfSe2	0.6715	-0.3256	5.542
HfTe2	0.0112	-0.0001	4.668
HfSeTe	0.0625	-0.0522	4.725
HfSTe	0.0558	-0.0470	4.582
ZrS2	1.4724	-0.3141	6.699
ZrSe2	0.4744	-0.3630	5.686
ZrTe2	0.0214	-0.0033	4.783
PtTe2	0.6708	-0.2519	4.641
PtS2	2.3626	-0.2800	6.779
PtSe2	1.5726	-0.2782	5.809
PtSTe	1.1280	-0.2510	6.322
SnS2	2.1252	-0.2643	7.084
SnSe2	1.0514	-0.3020	6.161
SnTe2	0.0238	-0.0100	5.122
SnSSe	1.2484	-0.2615	6.353
SnSTe	0.0056	-0.0020	5.162
SnSeTe	0.1205	-0.1160	5.526
NiS2	0.6820	-0.2197	5.729

Materials	CBM (eV)	VBM (eV)	WF (eV)
NiSe2	0.1722	-0.1593	4.968
NiTe2	0.0126	-0.0262	4.600
NiSeTe	0.0098	-0.0060	5.391

Table S2. ML-predicted data of the test set.

Materials	CBM	VBM	WF
ZrSTe	0.0469	-0.0650	4.630
ZrSeTe	-0.0283	-0.1083	4.725
PdSeTe	0.2033	-0.1411	5.308
PtSSe	1.7438	-0.2689	6.228

Table S3. DFT-computed data of the test set.

Materials	CBM	VBM	WF
ZrSTe	0.0781	-0.0615	4.729
ZrSeTe	0.0081	-0.1242	4.809
PdSeTe	0.3616	-0.2570	5.326
PtSSe	1.9275	-0.294	6.556

Table S4. ML-predicted values and DFT-calculated values of CBM, VBM, and WF.

	CBM	VBM	WF
ML-predicted values (eV)	0.7372	-0.2937	6.102
DFT-calculated values (eV)	0.8639	-0.2893	5.959

Table S5. The interlayer distances of g-SiC/SZrSe and g-SiC/SeZrS heterostructures.

heterostructures	Se-C (Å)	S-C (Å)	Bridge (Å)	Zr-C (Å)
g-SiC/SZrSe	3.1799	3.1744	3.1730	3.2006
g-SiC/SeZrS	3.1752	3.2333	3.2462	3.2427

The optical absorption coefficient (α(ω)) can be expressed as:[5]

$$\alpha(\omega) = \sqrt{2}\omega\left[\sqrt{\varepsilon_1^2(\omega) + \varepsilon_2^2(\omega)} - \varepsilon_1(\omega)\right]^{\frac{1}{2}} \quad (1)$$

where ω represents the frequency of the incident light, and ε_1 and ε_2 correspond to the real and imaginary parts of the derived complex dielectric function, respectively.

The STH efficiency can be calculated via the equation below:[6]

$$\eta_{STH} = 0.5 \times \frac{\Delta G \int_E^{\infty} \frac{P(\hbar\omega)}{\hbar\omega} d(\hbar\omega)}{\int_0^{\infty} P(\hbar\omega) d(\hbar\omega)} \quad (2)$$

where E is the bandgap of the material, ΔG is the potential difference of 1.23 eV for water splitting, and P($\hbar\omega$) is the AM1.5 solar energy flux at the photon energy $\hbar\omega$. The factor of 0.5 accounts for the fact that in the context of photocatalytic water splitting,

only half of the photogenerated carriers are converted into hydrogen energy.

References

[1] D. Li, W. Luo, X. Wei, Y. Zhang, Y. Yang, J. Liu, Y. Tian, L. Duan, Hydrogen production from photocatalytic water splitting in the InP/SnS2 heterojunction: First-principles calculations, Chem. Phys., 598 (2025) 112840.
[2] L. Feng, Q. Xiao, S. Li, F. Ai, L. Zhang, J. Ye, Q. Xie, First-principles study on SnC/GeS heterojunction as A direct Z-scheme photocatalyst for water splitting, Int. J. Hydrogen Energy, 193 (2025) 152393.
[3] D.D. Cheng, Y. Zhang, Y.Y. Jia, H.R. Zhu, Y.D. Feng, L. Duan, First-principles prediction of a novel 2D InAs/PtSe2 direct Z-scheme van der Waals heterojunction for overall water-splitting, Surf Sci., 761 (2025) 122798.
[4] J. Ren, J. Zhang, B. Tian, Z. Pan, S. Wang, H. Chen, K. He, H. Zhong, Q. Wang, First-principles study of the electronic, optical adsorption, and photocatalytic water-splitting properties of a strain-tuned SiC/WS2 heterojunction, Int. J. Hydrogen Energy, 87 (2024) 554-565.
[5] X. Huang, T.R. Paudel, S. Dong, E.Y. Tsymbal, Hexagonal rare-earth manganites as promising photovoltaics and light polarizers, PHYS REV B, 92 (2015) 125201.
[6] C.-F. Fu, J. Sun, Q. Luo, X. Li, W. Hu, J. Yang, Intrinsic Electric Fields in Two-dimensional Materials Boost the Solar-to-Hydrogen Efficiency for Photocatalytic Water Splitting, Nano Lett., 18 (2018) 6312-6317.